



3 4456 0268427 2

ORNL/TM-10612

oml

OAK RIDGE
NATIONAL
LABORATORY

MARTIN MARIETTA

Influence of Fast Alpha Diffusion and Thermal Alpha Buildup on Tokamak Reactor Performance

N. A. Ukan
J. S. Tolliver
W. A. Houlberg
S. E. Attenberger

OAK RIDGE NATIONAL LABORATORY
CENTRAL RESEARCH LIBRARY
CIRCULATION SECTION
OAK RIDGE, TN
LIBRARY LOAN COPY
DO NOT TRANSFER TO ANOTHER PERSON
If you wish someone else to see this
report, send in name with report and
the library will arrange a loan.
100-10612 1-1-77

OPERATED BY
MARTIN MARIETTA ENERGY SYSTEMS, INC.
FOR THE UNITED STATES
DEPARTMENT OF ENERGY

Printed in the United States of America. Available from
National Technical Information Service
U.S. Department of Commerce
5285 Port Royal Road, Springfield, Virginia 22161
NTIS price codes—Printed Copy A65 Microform A61

This report was prepared as an account of work sponsored by or for a agency of the United States Government. Neither the United States Government nor any agency thereof, nor any of their employees, makes any warranty, express or implied, or assumes any legal liability or responsibility for the accuracy or completeness, or usefulness of any information, apparatus, product, or process disclosed, or represents that its use would not infringe privately owned rights. Reference herein to any specific commercial product, process, or service by trade name, trademark, manufacturer, or otherwise, does not necessarily constitute or imply its endorsement, recommendation, or favoring by the United States Government or any agency thereof. The views and opinions of individuals expressed herein do not necessarily state or reflect those of the United States Government or any agency thereof.

**INFLUENCE OF FAST ALPHA DIFFUSION AND THERMAL ALPHA BUILDUP
ON TOKAMAK REACTOR PERFORMANCE**

N. A. Uckan
J. S. Tolliver*
W. A. Houlberg
S. E. Attenberger*

Presented at the Workshop on Alpha Particle Effects in ETR, Germantown, Maryland,
June 15-16, 1987
Proceedings to be published in *Fusion Technology*

Date published—November 1987

*Computing and Telecommunications Division, Martin Marietta Energy Systems, Inc.

Prepared by the
OAK RIDGE NATIONAL LABORATORY
Oak Ridge, Tennessee 37831
operated by
MARTIN MARIETTA ENERGY SYSTEMS, INC.
for the
U.S. DEPARTMENT OF ENERGY
under contract DE-AC05-84OR21400



3 4456 0268427 2

CONTENTS

ABSTRACT	v
I. INTRODUCTION	1
II. CLASSICAL THERMALIZATION	4
II. A. Slowing-Down Time	4
II. B. Fast Alpha Density and Beta	5
III. ANOMALOUS FAST ALPHA DIFFUSION	9
III.A. Threshold for Spatial Diffusion	9
III.B. Radial Transport Simulations	9
III.C. Discussion of Results	11
IV. THERMAL ALPHA BUILDUP	19
IV.A. Threshold for Thermal Alpha (Ash) Buildup	19
IV.B. Global Analysis	21
IV.C. Discussion of Results	22
V. SUMMARY	25
REFERENCES	27

ABSTRACT

The effect of fast alpha diffusion and thermal alpha accumulation on the confinement capability of a candidate Engineering Test Reactor (ETR) plasma [Tokamak Ignition/Burn Experimental Reactor (TIBER-II)] in achieving ignition and steady-state driven operation has been assessed using both global and 1-1/2-D transport models. Estimates are made of the threshold for radial diffusion of fast alphas and thermal alpha buildup. It is shown that a relatively low level of radial transport, when combined with large gradients in the fast alpha density, leads to a significant radial flow with a deleterious effect on plasma performance. Similarly, modest levels of thermal alpha concentration significantly influence the ignition and steady-state burn capability.

I. INTRODUCTION

Extensive reviews of alpha particle effects in tokamak plasmas are given in Refs. [1,2]. This paper summarizes studies of the influence of fast alpha diffusion and thermal alpha buildup on tokamak reactor performance.

In Sec. II, simple analytic expressions are developed for slowing-down time, fast alpha density, and beta. Estimates are made of the threshold for radial diffusion (Sec. III) and thermal alpha buildup, along with thermal alpha equilibrium concentration (Sec. IV). The results are then applied to a representative ETR [3] (TIBER-II [4]) plasma. Specifically, the effect of fast alpha diffusion (Sec. III) and thermal alpha accumulation (Sec. IV) on the confinement capability of TIBER-II in achieving ignition and steady-state driven operation has been assessed using both global [5–7] and 1-1/2-D (WHIST [8,9]) transport models. Parameters used are summarized in Table I. Physics models and assumptions considered in these studies are compiled in Table II. Here the confinement assumptions are those developed for the Compact Ignition Tokamak (CIT) [5,6,10,11]. Details of the confinement scalings [12–15] and operational limits [16–18] are given in the references.

It is shown in Sec. III that a relatively low level of radial transport, when combined with large gradients in the fast alpha density, leads to a significant radial flow with a deleterious effect on plasma performance due to broadening of heating profile. Similarly, in Sec. IV, modest levels of thermal alpha concentration are shown to significantly influence the ignition and steady-state burn capability.

TABLE I
TIBER-II Machine and Plasma Parameters

Design Parameters [4]	
Major radius, R_0 (m)	3.0
Minor radius, a (m)	0.834
Elongation, κ	2.22
Triangularity, δ	0.4
Toroidal field, B_0 (T)	6.0
Plasma current, I (MA)	10.0
Calculated Parameters [7,16-18]	
Cylindrical q , q_*	2.5
Density limit (10^{20} m^{-3})	
Murakami, $\langle n_{mu} \rangle = 1.5B_0/R_0q_*$	1.2
Greenwald, $\langle n_{GR} \rangle = 0.6I/\pi a^2$	2.75
Troyon beta limit ($\beta_{crit} \approx 3I/aB_0$ %)	6.0

TABLE II
Physics Models [5–20]

<u>Radial Profiles:</u>	$x = x_0(1 - r^2/a^2)^{\alpha_x}$; $x = n, T$ (and J)
in global model:	$\alpha_n = 0.5$; $\alpha_T = 1.0$; $\alpha_J = 3 \alpha_T/2 = 1.5$
in WHIST code:	$\alpha_n = 0.5$; $\alpha_T =$ transport determined; $\alpha_J =$ fixed to maintain $q(0) \geq 1$
<u>Effective Charge</u> (if specified):	$Z_{\text{eff}} = 1.5$ (made up with carbon impurities)
<u>Confinement Scalings:</u>	$(1/\tau_E)^2 = (1/\tau_{\text{EOH}})^2 + (1/\tau_{\text{Eaux}})^2$ with $\tau_{\text{EOH}} = \tau_{\text{ENA}}$; $\tau_{\text{Eaux}} = \tau_{\text{EKG}}$
Neo-Alcator (Ref. 12):	$\tau_{\text{ENA}} = 0.07 \langle n_{20} \rangle a R_0^2 q_*$
Kaye-Goldston (L-mode $f_L = 1$, H-mode $f_L = 2$) (Ref. 13):	$\tau_{\text{EKG}} = 0.056 f_L^{1.24} (P_{\text{heat}})^{-0.58} R_0^{1.65} a^{-0.49} \kappa^{0.28} \langle n_{20} \rangle^{0.26} B^{0.09} (A_i/1.5)^{0.5}$ in global model: $\tau_{\text{Ee}} = \tau_{\text{Ei}} = \tau_E$ (e.g., $\chi_e \approx \chi_i \approx \chi_{\text{KG+NA}} \sim C a^2 / \tau_E$; $C \sim 0.3-0.4$) in WHIST code: $\chi_e = g(\rho) \chi_{\text{KG+NA}}$; $\chi_i = \chi_{\text{iNC}} + 0.2 \chi_e$; $D = D_{\text{NC}} + 0.2 \chi_e$ $\chi_{\text{KG+NA}}$ = anomalous electron thermal diffusivity (see global model) χ_{iNC} = ion neoclassical thermal diffusivity (Refs. 14,15) D_{NC} = neoclassical particle diffusivity $g(\rho) = [1 + 4(\rho/a)^2]/2$, profile shape factor
<u>Units/Definitions:</u>	(mks, MA, MW, keV, $n_{20} = n_e/10^{20}$; $T_{10} = T/10$)
(Elliptic) Cylindrical q :	$q_* \approx (5a^2 B_0 / I R_0) [1 + \kappa^2 (1 + 2\delta^2 - 1.2\delta^3)]/2$ (Refs. 5–7)
Enhancement factors:	$f_L =$ L-mode enhancement factor; $A_i = 2.5$ (average D-T atomic mass)
Power degradation:	$P_{\text{heat}} =$ (ohmic + alpha + auxiliary – radiation) power

II. CLASSICAL THERMALIZATION

II.A. Slowing-Down Time

The classical alpha slowing-down time, $\tau_{s\alpha}$, is [1,19]

$$\tau_{s\alpha} = - \int dE_{\alpha} / (dE_{\alpha}/dt) = (2\tau/3) \ln[1 + (E_{\alpha 0}/E_{\text{crit}})^{3/2}], \quad (1)$$

where $E_{\alpha 0} = 3.52$ MeV, the alpha birth energy. The characteristic relaxation time for energy exchange, τ , and critical energy for alpha particles in a 50-50 D-T plasma are given by (in mks units with temperatures and energies in kilo electron volts)

$$\begin{aligned} \tau &= (2\pi)^{1/2} 3\pi\epsilon_0^2 m_{\alpha} (kT_e)^{3/2} / (m_e^{1/2} n_e Z_{\alpha}^2 e^4 \ln\Lambda) \\ &\approx 10^{19} T_e^{3/2} / (n_e \ln\Lambda) \approx 0.19 (T_{e10})^{3/2} / n_{e20}, \end{aligned} \quad (2)$$

$$E_{\text{crit}} \approx 14.8 A_{\alpha} T_e [\sum (n_i Z_i^2 \ln\Lambda_i / A_i) / n_e \ln\Lambda_e]^{2/3}. \quad (3)$$

Here, the summation is over all ion species ($i = \text{D, T, } \alpha, \text{ impurities}$), $T_{e10} = T_e/10$ keV, and $n_{e20} = n_e/10^{20} \text{ m}^{-3}$. For $Z_{\text{eff}} \sim 1.5$ (assuming $\ln\Lambda_i \sim \ln\Lambda_e$), $E_{\text{crit}} \sim 33.5 T_e$ and typical slowing-down times are given in Table III. [Here $Z_{\text{eff}} = \sum (n_i Z_i^2) / n_e$ is the effective charge.] Note that $\tau_{s\alpha}$ is inversely proportional to n_e and is nearly proportional to T_e due to the fact that $\ln[1 + (E_{\alpha 0}/E_{\text{crit}})^{3/2}] \sim C/T_e^{1/2}$, where C ($\sim 11 \pm 1$) is nearly a constant. Operation at high n_e and low T_e , characteristic of CIT [11], reduces $\tau_{s\alpha}$. Operation at moderate to low n_e and moderate to high T_e , characteristic of the International Thermonuclear Experimental Reactor (ITER)/TIBER [3,4], increases $\tau_{s\alpha}$. In this (low n_e , high T_e) regime, $\tau_{s\alpha}$ can be relatively long, often exceeding projected energy (τ_E) and particle (τ_p) confinement times for thermal (D-T) plasmas.

TABLE III
Classical Alpha Slowing-Down Time (Local Values)

T_e (keV)	$n_e / (10^{20} \text{ m}^{-3})$						
	0.5	1.0	2.0	3.0	5.0	7.0	10.0
5	0.4	0.2	0.1	0.07	0.04	0.03	0.02
10	0.9	0.45	0.23	0.15	0.09	0.065	0.045
20	1.8	0.9	0.45	0.31	0.18	0.13	0.09
30	2.7	1.35	0.68	0.45	0.27	0.19	0.135
40	3.4	1.7	0.85	0.57	0.34	0.24	0.17
50	4.0	2.0	1.0	0.67	0.4	0.29	0.2

II.B. Fast Alpha Density and Beta

Classical thermalization leads to a fast alpha density, $n_{f\alpha}$, given as

$$n_{f\alpha} = n_D n_T \langle \sigma v \rangle_{DT} \tau_{s\alpha}. \quad (4)$$

If we normalize to n_e and assume a 50-50 D-T plasma, then

$$n_{f\alpha}/n_e = (n_e \tau_{s\alpha}) (f_{DT}^2 \langle \sigma v \rangle_{DT} / 4), \quad (5)$$

where $f_{DT} = (n_D + n_T)/n_e \sim 0.9$ for $Z_{\text{eff}} \sim 1.5$.

An average energy for the fast alphas is

$$\begin{aligned} \langle E_{f\alpha} \rangle / E_{\alpha 0} &\approx (\tau / \tau_{s\alpha}) U_{\alpha e} \\ &\approx (3U_{\alpha e} / 2) / \ln[1 + (E_{\alpha 0} / E_{\text{crit}})^{3/2}]. \end{aligned} \quad (6)$$

Here, $U_{\alpha e}$ is the fraction of alpha energy given to the electrons. For most energy ranges of interest, collisions with the electrons are dominant, and electron heating exceeds ion heating by a significant amount. Any processes, however, that lead to anomalously fast thermalization are likely to be beneficial [9] because they would improve ion heating and might reduce the impact of radial diffusion (discussed in Sec. III). For local T_e values up to about 100 keV, an approximate fit to $U_{\alpha e}$ is given by [20]

$$U_{\alpha e} \approx 1 - (T_e/50) + 0.37(T_e/50)^{7/4} . \quad (7)$$

A contribution from these fast alphas to the total plasma pressure can be relatively high (~10–30%) for fusion temperatures of interest. Because the maximum volume-averaged beta $\langle\beta_{tot}\rangle$ achievable in a tokamak is limited by magnetohydrodynamic (MHD) instabilities (e.g., ballooning and kink modes), the presence of fast alphas, if $\langle\beta_{tot}\rangle = \text{const}$, reduces the background thermal plasma pressure. Furthermore, the energetic alpha population can influence (favorably or unfavorably) the bulk plasma ballooning mode stability boundaries. As shown in Ref. [21], alphas in the energy range with $\langle E_{f\alpha}\rangle/T_i < 150$ are the most destabilizing energy group. Here, the influence of fast alphas on stability boundaries (i.e., on the maximum stable $\langle\beta_{tot}\rangle = \langle\beta_e + \beta_i + \beta_{f\alpha}\rangle$ value) has not been considered, though their contribution to the total pressure is taken into account. The fast alpha beta is

$$\beta_{f\alpha} = (2n_{f\alpha}\langle E_{f\alpha}\rangle/3)/(B_o^2/2\mu_o) . \quad (8)$$

Normalizing to plasma thermal beta $\beta_{th} = \beta_e + \beta_i$ (here i refers to all thermal ion species) yields

$$\beta_{f\alpha}/\beta_{th} = (2E_{\alpha 0}/3T_e)(n_{f\alpha}/n_e)(\langle E_{f\alpha}\rangle/E_{\alpha 0})/(1 + f_{nT}) , \quad (9)$$

where $f_{nT} = f_n f_T = (n_i/n_e)(T_i/T_e)$. For $T_i \sim T_e \sim T$ and $Z_{\text{eff}} \approx 1.5$ (with $Z = 6$, carbon), $f_{nT} \sim 0.9$ and typical local values of fractional fast alpha density, beta, and energy are given in Table IV. Note that fractional contributions ($n_{f\alpha}/n_e$, $\beta_{f\alpha}/\beta_{\text{th}}$, $\langle E_{f\alpha} \rangle / E_{\alpha 0}$) depend only on temperature (T_e and T_i/T_e ; the latter is assumed to be unity in Table IV).

TABLE IV
Fast Alpha Density and Beta (Local Values)

T (keV)	$\langle \sigma v \rangle_{DT}$ (m^3/s)	$n_{f\alpha}/n_e$ (%)	$\beta_{f\alpha}/\beta_{\text{th}}$ (%)	$\langle E_{f\alpha} \rangle / E_{\alpha 0}$
5	$1.35(10^{-23})$	0.01	0.73	0.3
10	$1.13(10^{-22})$	0.1	4.2	0.34
20	$4.31(10^{-22})$	0.8	19	0.39
30	$6.65(10^{-22})$	1.8	31	0.41
40	$7.93(10^{-22})$	2.7	34	0.41
50	$8.54(10^{-22})$	3.45	34	0.4

In global power balance calculations, one is interested in the volume-averaged quantities. Profile effects can be accounted for in a simple fashion by considering profiles of the form $x = x_0(1 - r^2/a^2)^{\alpha_x}$, where $x = n, T$. For $\alpha_n \sim 0-0.5$ (relatively flat density profile) and $\alpha_T \sim 1.0$ (nearly parabolic temperature profiles), Eq. (9) yields [20]

$$\begin{aligned} \gamma_{f\alpha} = \langle \beta_{f\alpha} \rangle / \langle \beta_{\text{th}} \rangle &\approx 0.32 f_{DT}^2 (T_i/T_e)^2 \langle T_{e10} \rangle^{5/2} \langle U_{\alpha e} \rangle / (1 + f_{nT}) \\ &= 0.32 f_{DT}^2 (T_i/T_e)^2 \langle T_{10} \rangle^{5/2} \langle U_{\alpha e} \rangle [2^{5/2} / (1 + f_{nT})^{7/2}], \end{aligned} \quad (10)$$

where $\langle T \rangle = \langle n_e T_e + n_i T_i \rangle / \langle 2n_e \rangle = \langle T_e \rangle (1 + f_{nT}) / 2$ is the density-weighted average temperature. For analytical simplicity, in Eq. (10) $\langle \sigma v \rangle_{DT}$ (the fusion reaction-rate parameter) is approximated as $\langle \sigma v \rangle_{DT} \approx 1.1 \times 10^{-22} (T_{i10})^2$, which is accurate enough for $T \sim 7\text{--}20$ keV. For the chosen profiles and $Z_{\text{eff}} \sim 1.5$, the average pressure contribution from fast alphas is $\gamma_{f\alpha} \sim 5\text{--}20\%$ for $\langle T \rangle \sim 6\text{--}15$ keV. Direct comparison between the predictions of Eq. (10) and a large number of 1-1/2-D WHIST transport code calculations (having similar profile shapes and Z_{eff} values) shows good agreement (within $\pm 15\%$) over the temperature range ($\langle T \rangle \sim 5\text{--}20$ keV) considered. A benchmark between Eq. (10) and WHIST has resulted in a simple functional fit [20] that is more convenient to use in global analyses:

$$\gamma_{f\alpha} \approx 0.2(\langle T_{10} \rangle - 0.37) \quad \text{for } Z_{\text{eff}} \sim 1.5, T_i/T_e \sim 1, \langle T \rangle \sim 5\text{--}20 \text{ keV.} \quad (11)$$

To zeroth order, the assumption of different profiles ($\alpha_n \sim 0\text{--}1.0$, $\alpha_T \sim 0.5\text{--}2.0$) did not appear to have any significant effect on this simple fit. As expected, significant deviations from Eq. (11) were seen in simulations for anomalous fast alpha diffusion and energy relaxation. In such cases, however, global analysis is not adequate to describe the fast alpha behavior. The WHIST code calculations are used in Sec. III. Equation (11) is used in Sec. IV and in Refs. [5–7].

III. ANOMALOUS FAST ALPHA DIFFUSION

III.A. Threshold for Spatial Diffusion

Classical models predict strong central peaking of fast alpha density [see Eq. (4) and Table IV]. Such large gradients in $n_{f\alpha}$ can lead to significant radial flow in the presence of an anomalous diffusion. Radial transport becomes important when [9]

$$\tau_{p\alpha} \approx (a_{\text{eff}})^2/4D_{\alpha} \leq \tau_{s\alpha}, \quad (12)$$

where $\tau_{p\alpha}$ is the fast alpha diffusion time. The threshold value for the diffusion coefficient is

$$D_{\alpha} \geq (a_{\text{eff}})^2/4\tau_{s\alpha} \approx (a/2)^2/4\tau_{s\alpha}. \quad (13)$$

Here $a_{\text{eff}} \approx a/2$ is taken because of the centralized nature of the fast alpha concentration. In TIBER-II ($a = 0.84$ m) with a 50-50 D-T plasma, the fast alpha confinement time is shorter than the slowing-down time when $D_{\alpha} \geq 0.1n_{20}/T_{10}$ (m^2/s), where $\tau_{s\alpha}$ [see Eqs. (1)–(3) and Table III] is approximated as $\tau_{s\alpha} \sim 0.45T_{10}/n_{20}$. For $n_e \sim (1-2)10^{20} \text{ m}^{-3}$ and $T \sim 10-20$ keV, radial transport becomes important if $D_{\alpha} \geq 0.05-0.2 \text{ m}^2/\text{s}$. These values are comparable to the thermal particle diffusion coefficient, $D = a^2/4\tau_p = a^2/20\tau_E = 0.04n_{20}/(n_{20}\tau_E)$. (Here $\chi = 5D$, or $\tau_p = 5\tau_E$, is assumed.)

III.B. Radial Transport Simulations

The 1-1/2-D WHIST transport code has been used to examine the sensitivity of performance in TIBER-II plasmas to radial diffusion of fast alpha particles. The physics

models used are given in Table II and are briefly summarized here. The transport model assumed an electron heat conductivity χ_e given by a combination of Kaye-Goldston [13] and neo-Alcator [12,13] scaling, $\chi_e = \chi_{KG+NA}$. The Chang-Hinton formulation [14] (with Hirshman-Sigmar trapping fractions [15]) for ion neoclassical conductivity was used and a portion (20%) of the anomalous χ_e was added to the ions (instead of using a neoclassical multiplier), $\chi_i = 0.2\chi_e + \chi_{NC}$. The density profile was governed by a balance between neoclassical plus anomalous diffusivity and an empirical inward convective flux that was automatically adjusted to force the density profile toward a square-root-parabolic shape. The external gas feed rates were feedback-controlled to give 50-50 D-T (volume average) densities. The current density profile was frozen and $q(0) > 1$ was enforced; thus, sawtooth activity was not triggered. The temperature profile was decoupled from the ohmic relation to the current profile in an effort to accommodate the TIBER-II mission [4] of noninductive current drive, though no effort was made to model the current drive self-consistently. Thermalized alphas were not retained in the plasma. $Z_{eff} = 1.5$ was maintained with carbon as the only impurity.

A Gaussian heating profile with a 0.4-m half-width was used to simulate the ion cyclotron resonant frequency (ICRF) heating. The division of power between electrons and ions was taken as 25%/75%. Although this assumption has no real effect on the results at high densities (because of tight coupling between thermal electrons and ions), at lower densities a decoupling may occur that drives the electron and ion temperatures apart. (Especially in density-temperature regimes where $\tau_{Ei} \gg \tau_{Ee}$, T_i/T_e may increase strongly with temperature.)

A multienergy group model [9] was used for radial diffusion of the fast alpha particles with a classical model for collisional energy relaxation on the background thermal electrons and ions. The simplest form for the radial fast particle flux for a given energy group j has the form

$$\Gamma_{\alpha j} = -D_{\alpha j} \langle |\nabla\rho|^2 \rangle (\partial n_{f\alpha j} / \partial \rho) , \quad (14)$$

where ρ is the radial coordinate that labels a flux surface and the flux-surface-averaged quantity $\langle |\nabla\rho|^2 \rangle = (1 + \kappa^2)/2\kappa^2$ provides a conversion to real space ($\kappa = b/a =$ elongation). In general, D_α will be a function of alpha particle energy, thermal plasma parameters, and magnetic geometry [1,2,9,19]. To illustrate the effects of fast alpha diffusion, we have chosen, for simplicity, $D_{\alpha j} = D_\alpha = \text{const}$ as a representation of the threshold value associated with excitation of various instabilities [1,2,8,22].

III.C. Discussion of Results

The steady-state fast alpha distribution function $f_\alpha(v,r)$ for a typical TIBER-II plasma (see Table I) is shown in Figs. 1 (H-mode) and 2 (L-mode) with $D_\alpha = 0, 0.2,$ and $0.5 \text{ m}^2/\text{s}$. For the case of classical local thermalization ($D_\alpha = 0$), the steady-state alpha distribution function, $f_\alpha(v) \sim S_\alpha \tau / [v^3 + (v_{\text{crit}})^3]$ with $S_\alpha = n_D n_T \langle \sigma v \rangle_{DT}$ and $E_{\text{crit}} = m_\alpha (v_{\text{crit}})^2/2$, monotonically decreases with velocity at all radii [1,19]. When radial diffusion at a level $D_\alpha = 0.2 \text{ m}^2/\text{s}$ is added, the distribution function develops a smaller gradient at high v . Further increases in radial diffusion ($D_\alpha \geq 0.5 \text{ m}^2/\text{s}$) nearly flatten the distribution function; eventually, inversion ($\partial f_\alpha / \partial v > 0$) could occur, especially for H-mode (Fig. 1). Inversion in L-mode requires somewhat higher (~50–60%) D_α values because the plasma thermal diffusion coefficient is higher in L-mode than in H-mode ($H = 2L$). (Note that the ratio is not 2 because of the τ_{ENA} term in τ_E , see Table II.) Thus, with radial fast alpha diffusion at a level comparable to the thermal particle diffusion, it is feasible to generate inversion of the steady-state fast alpha distribution function even if thermalization remains classical. This inversion may drive instabilities and may lead to anomalous thermalization, both of which may have desirable effects [1,2,9]. As discussed in Ref. [19], transient inversion of $f_\alpha(v,r,t)$ is also possible if the alpha particle source rate (or T_e , and therefore $\tau_{S\alpha}$) is increased too rapidly. Details of the transient inversion criterion are given in Ref.

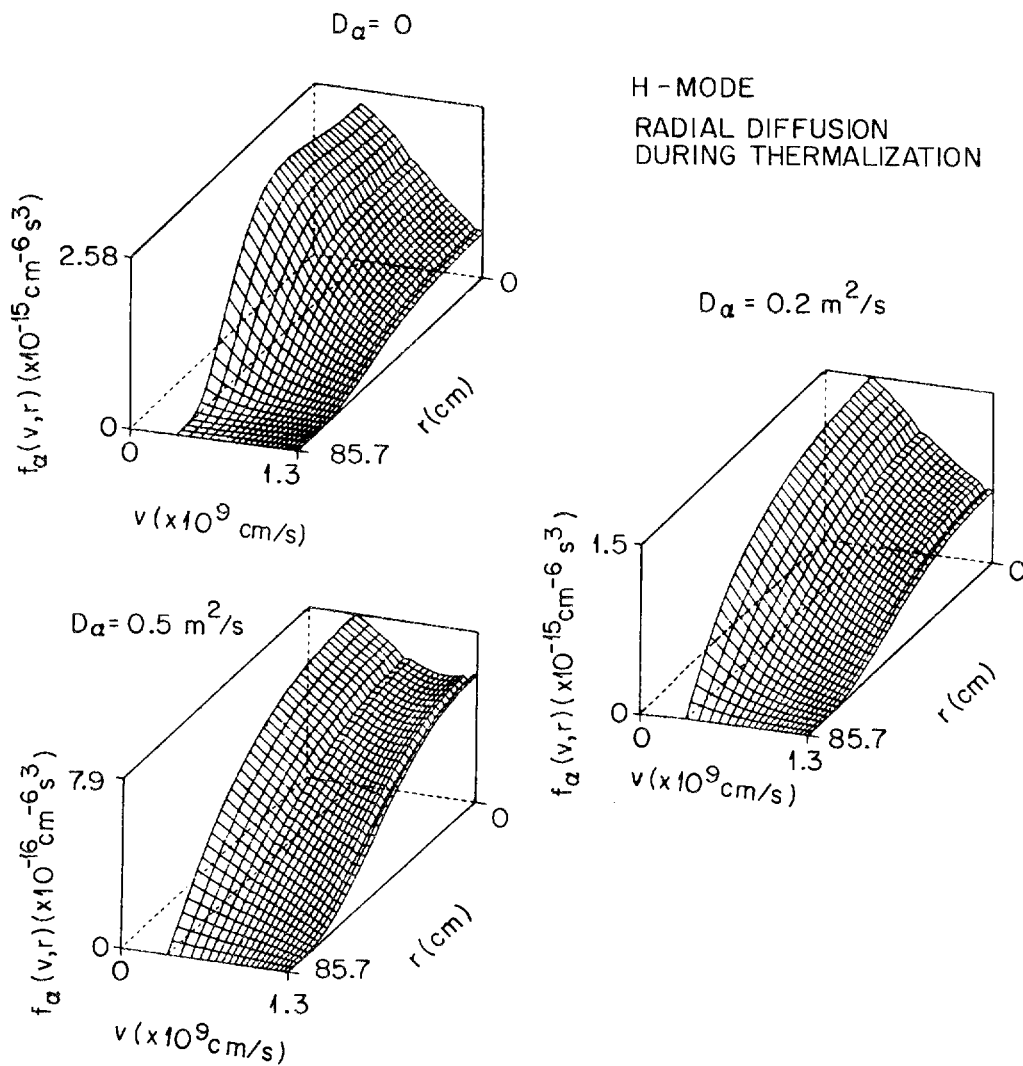


FIG. 1. The steady-state fast alpha distribution function $f_\alpha(v, r)$ in TIBER-II for H-mode scaling with $\langle n_e \rangle \sim 2.2 \times 10^{20} \text{ m}^{-3}$ and $D_\alpha = 0, 0.2, \text{ and } 0.5 \text{ m}^2/\text{s}$. $f_\alpha(v, r)$ monotonically decreases with velocity at all radii for $D_\alpha = 0$. Radial diffusion broadens $f_\alpha(v, r)$, in both v and r , and $D_\alpha \geq 0.5 \text{ m}^2/\text{s}$ may invert the distribution in v .

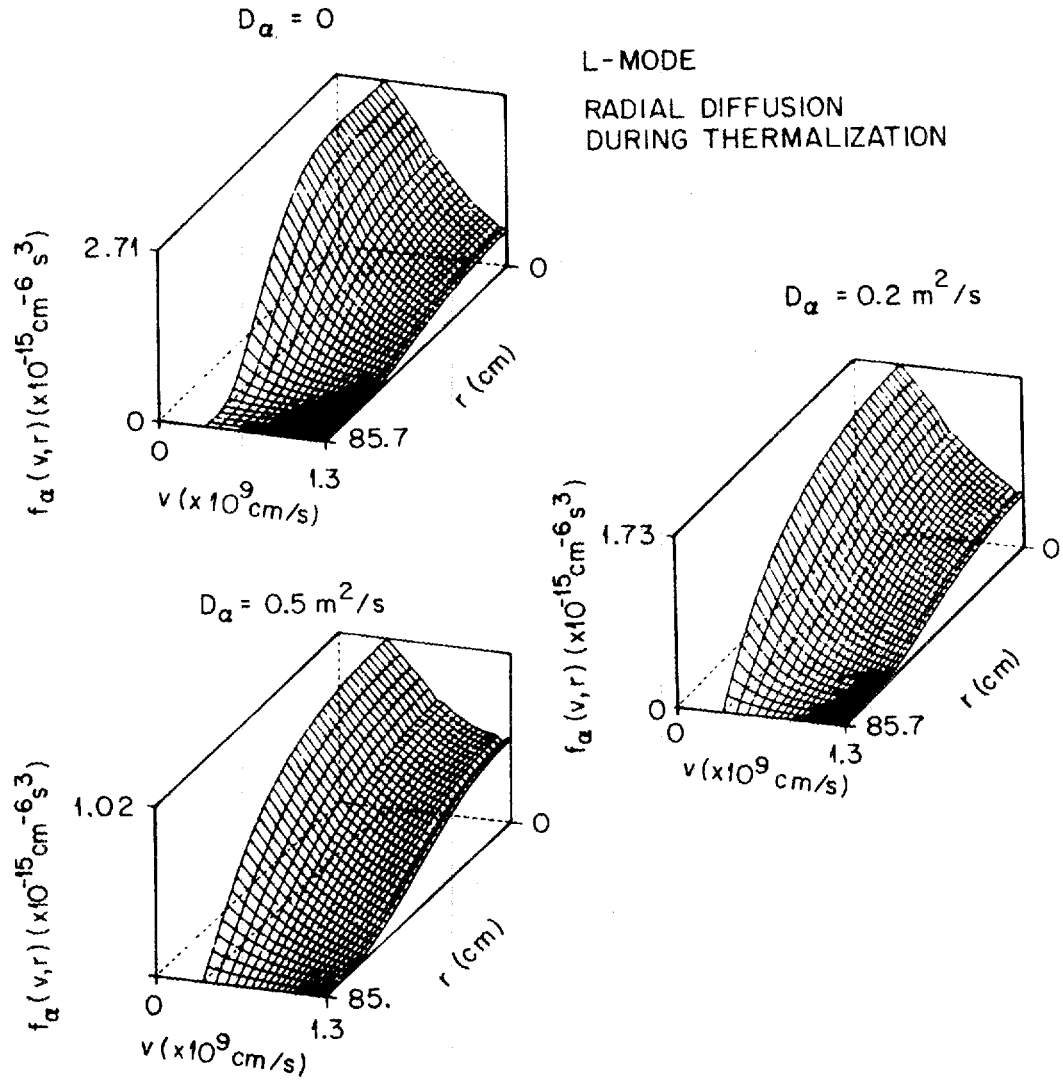


FIG. 2. The steady-state fast alpha distribution function $f_\alpha(v, r)$ in TIBER-II for L-mode scaling with $\langle n_e \rangle \sim 2.6 \times 10^{20} \text{ m}^{-3}$ and $D_\alpha = 0, 0.2, \text{ and } 0.5 \text{ m}^2/\text{s}$. General results are similar to Fig. 1, except that inversion of $f_\alpha(v, r)$ requires higher D_α .

[19], and the resulting instabilities that further affect the thermalization and spatial diffusion are reviewed in Refs. [1,2].

As evidenced from Figs. 1 and 2, radial diffusion broadens f_α and reduces its magnitude. As a consequence, the fast alpha population (n_α) and resulting fast alpha contribution to pressure ($\beta_{f\alpha}/\beta_{th}$) are significantly reduced, as illustrated in Figs. 3 and 4, respectively. Note that, for $D_\alpha = 0$, the magnitude and shape of the $\beta_{f\alpha}/\beta_{th}$ contours are consistent with the predictions of global analyses given in Sec. II. Namely, $\beta_{f\alpha}/\beta_{th} \sim 5\text{--}20\%$ for $\langle T \rangle \sim 6\text{--}15\text{ keV}$ and $\beta_{f\alpha}/\beta_{th} = f(T, T_i/T_e)$ only. At low densities ($\langle n_e \rangle \leq 10^{20}\text{ m}^{-3}$), however, a somewhat weaker coupling between electrons and ions

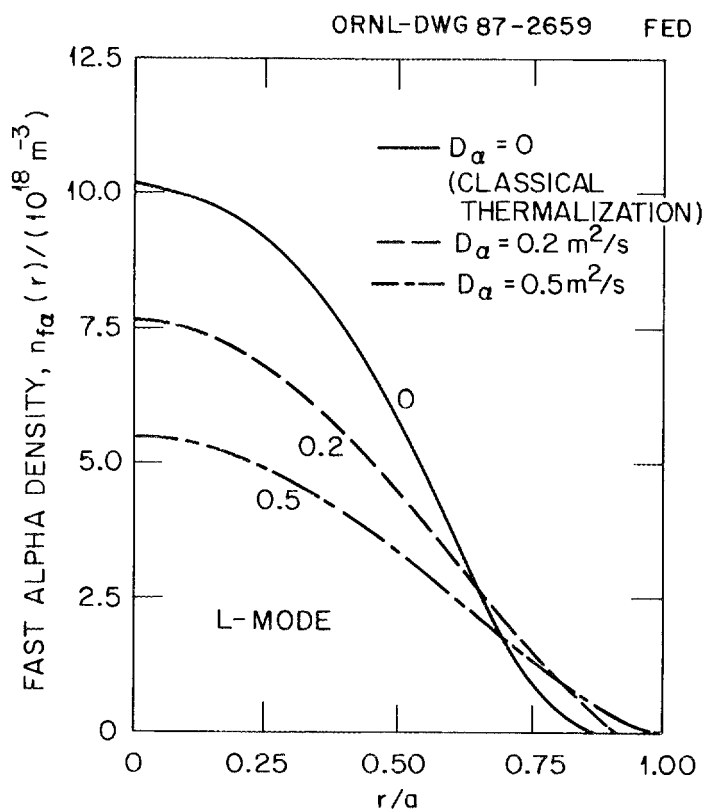


FIG. 3. Radial profiles of the fast alpha density (integrated over energy) for various levels of fast alpha diffusion ($D_\alpha = 0, 0.2, \text{ and } 0.5\text{ m}^2/\text{s}$) with an L-mode scaling in TIBER-II. Radial diffusion significantly reduces the fast alpha population and broadens its profile.

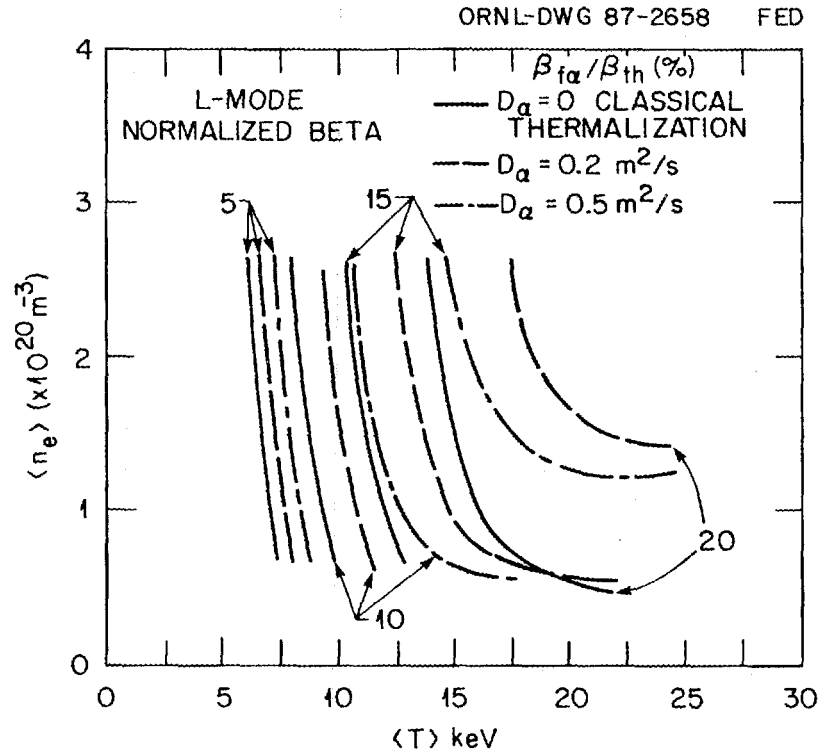


FIG. 4. The ratio of fast alpha pressure to thermal plasma pressure ($\langle \beta_{f\alpha} \rangle / \langle \beta_{th} \rangle$) for various levels of fast alpha diffusion ($D_\alpha = 0, 0.2, \text{ and } 0.5 \text{ m}^2/\text{s}$). In steady-state operation, $\langle \beta_{f\alpha} \rangle / \langle \beta_{th} \rangle$ is (at most) a weak function of density for classical local thermalization ($D_\alpha = 0$) in which the contours are representative of most reactor-grade plasmas, because the only sensitivity is to T_e and T_e/T_i and, to some degree, to density and temperature profile shapes. Radial diffusion significantly reduces the fast alpha contribution to the pressure.

results in $T_i/T_e = f(n)$, and in turn $\beta_{f\alpha}/\beta_{th} = f[T, T_i/T_e(n)]$. As expected, the cases for $D_\alpha = 0.2$ and 0.5 are significantly different.

Figure 5 shows the effect of increasing D_α on the ignition region for TIBER-II with Kaye-Goldston H-mode scaling. The results were generated by the WHIST code with the POPCON option by driving the time-dependent equations to equilibrium [8]. Reference

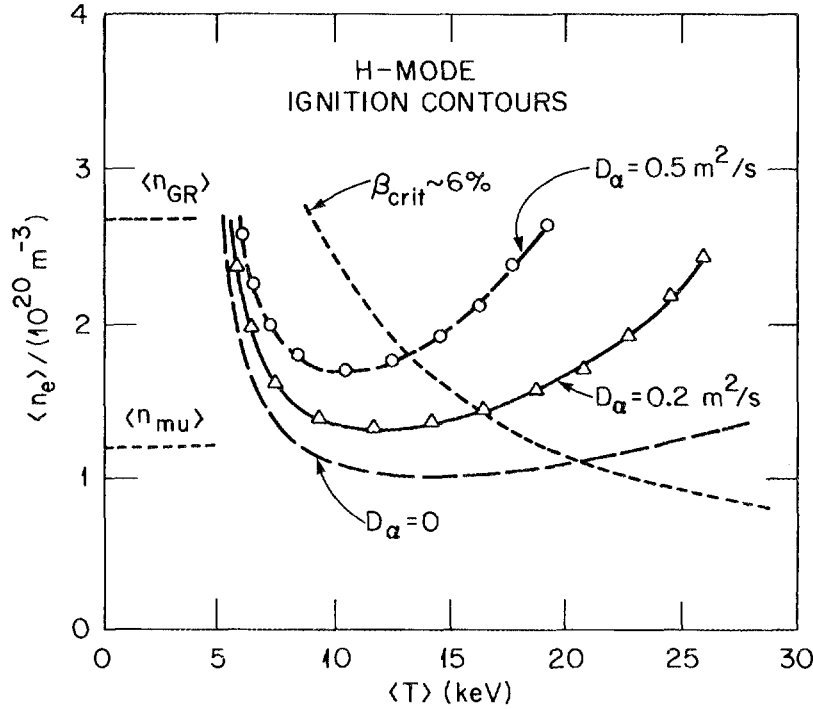


FIG. 5. Influence of fast alpha diffusion on ignition in TIBER-II with an H-mode scaling. Reference beta ($3I/aB_0 \sim 6\%$) and density ($\langle n_{20\mu} \rangle \sim 1.2$; $\langle n_{20GR} \rangle \sim 2.75$) limits are shown to indicate the extent of the operational boundaries. Radial diffusion moves the ignition contours to higher densities and reduces the size of the operating window.

beta and density limits [16–18] are also shown. An increase in radial diffusion moves the ignition contours to higher densities because of the broadening of the heating profile. For this H-mode case, at densities below the Murakami limit [12,16], there is a small ignition window for $D_\alpha = 0$, which is eliminated if $D_\alpha > 0.1 \text{ m}^2/\text{s}$. For higher density limits, such as $\langle n_{GR} \rangle$ [17], the ignition window still exists but is significantly reduced for $D_\alpha = 0.5 \text{ m}^2/\text{s}$.

The contours in Fig. 6 show the threshold for ignition and $Q = 20$ with the L-mode scaling. Note that the small ignition regime ($n_{GR} < n < n_{mu}$; $\beta < \beta_{crit}$) that existed for

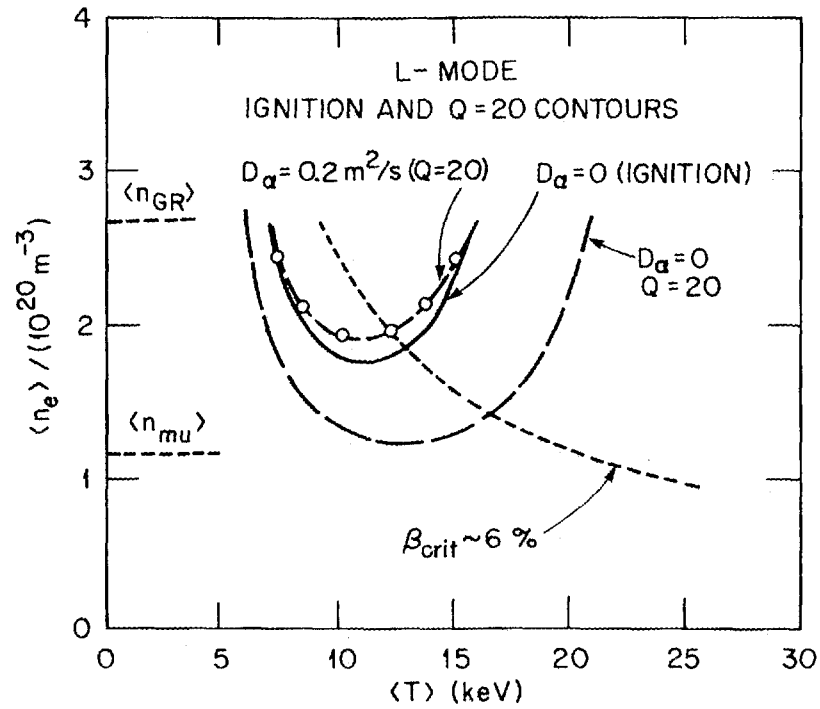


FIG. 6. Influence of fast alpha diffusion on ignition and $Q = 20$ contours in TIBER-II with an L-mode scaling. A small amount of radial diffusion with $D_\alpha \sim 0.1 \text{ m}^2/\text{s}$ eliminates the ignition region, independent of the density and beta limits shown. Similarly, the $Q = 20$ operating window is reduced with added diffusion and is eventually lost for $D_\alpha > 0.2 \text{ m}^2/\text{s}$.

$D_\alpha = 0$ is eliminated when a radial diffusion with $D_\alpha \approx 0.2 \text{ m}^2/\text{s}$ is added. The $Q = 20$ operating window is also reduced and is eventually eliminated if D_α is further increased. The influence of D_α on $Q = 10$ contours is shown in Fig. 7.

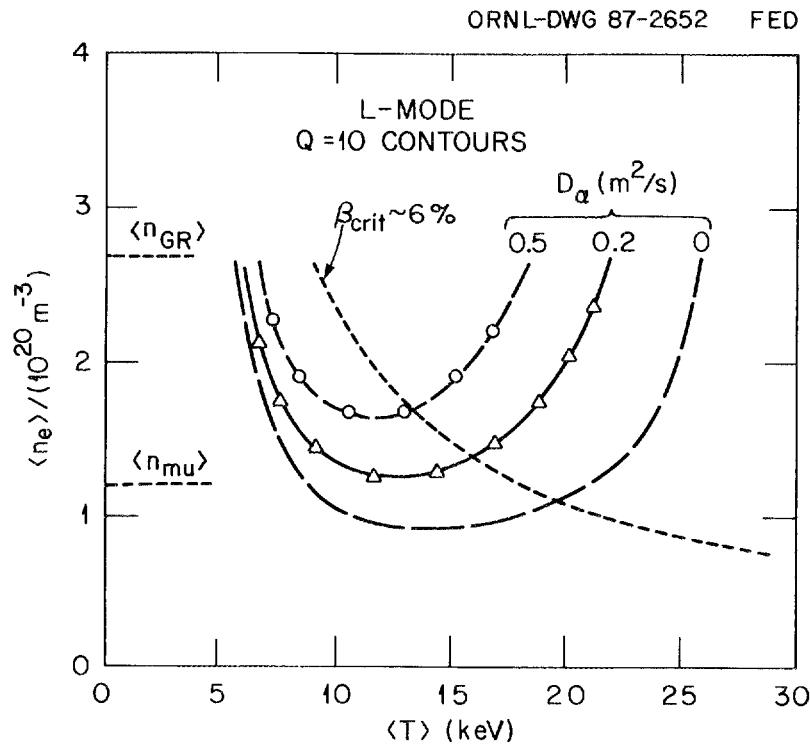


FIG. 7. Influence of fast alpha diffusion on $Q = 10$ contours in TIBER-II with L-mode scaling.

IV. THERMAL ALPHA BUILDUP

IV.A. Threshold for Thermal Alpha (Ash) Accumulation

Assuming classical local thermalization, the simplest form for the coupled particle balance equations for fast (average energy $\langle E_{f\alpha} \rangle$) and thermal (energy of $3T_i/2$) alphas is

$$\partial n_{f\alpha} / \partial t = S_{\alpha} - n_{f\alpha} / \tau_{s\alpha} = n_D n_T \langle \sigma v \rangle_{DT} - n_{f\alpha} / \tau_{s\alpha}, \quad (15a)$$

$$\partial n_{\alpha} / \partial t = n_{f\alpha} / \tau_{s\alpha} - n_{\alpha} (1 - R_{\alpha}) / \tau_p = n_{f\alpha} / \tau_{s\alpha} - n_{\alpha} / \tau_p^*, \quad (15b)$$

where n_{α} is the thermal alpha density, $\tau_p^* = \tau_p / (1 - R_{\alpha})$ is the effective thermal alpha particle confinement time with R_{α} the recycling rate [or $(1 - R_{\alpha})$ the pumping rate], and the other quantities are defined in Sec. II. Temporal and spatial evolutions are important, and solutions to Eq. (15) require time-dependent radial transport calculations. In general, the particle transport is not well understood, and results obtained are model dependent.

Here we develop several simplified expressions that can give some insights into questions such as "How fast do the thermal alphas accumulate?", "What is the burn pulse length if $R_{\alpha} = 1$ (perfect recycling)?", "What is the required recycling rate to maintain an equilibrium concentration below some threshold value?", etc. Because the time scale associated with classical thermalization is shorter than the characteristic times for thermal alpha buildup and τ_p^* , Eq. (15) reduces to

$$\partial n_{\alpha} / \partial t = n_{f\alpha} / \tau_{s\alpha} - n_{\alpha} / \tau_p^* = n_D n_T \langle \sigma v \rangle_{DT} - n_{\alpha} / \tau_p^*. \quad (16)$$

By normalizing to n_e and assuming a 50-50 D-T plasma with no impurities, except helium ash, we obtain

$$\partial f_{\alpha}/\partial t = (n_{f\alpha}/n_e)/\tau_{s\alpha} - f_{\alpha}/\tau_{p^*} = (1 - 2f_{\alpha})^2(n_e\langle\sigma v\rangle_{DT}/4) - f_{\alpha}/\tau_{p^*}, \quad (17)$$

where $f_{\alpha} = n_{\alpha}/n_e$ and $f_{DT} = (n_D + n_T)/n_e = 1 - 2f_{\alpha}$. If the heating of the plasma to fusion temperatures is instantaneous (or if the heating time is much shorter than the time scales of interest for ash buildup), such that the temperature $\langle T \rangle$ is constant during the burn phase, Eq. (17) can be integrated analytically [23] (if n_e is held constant). For $K = C\tau_{p^*} = (n_e\tau_{p^*})(\langle\sigma v\rangle_{DT}/4) = \text{const}$ and $f_{\alpha}(t = 0) = 0$, the solution is

$$f_{\alpha}(t) = n_{\alpha}/n_e = 1/2 + 1/8K - [(1 + 8K)^{1/2}/8K]\tanh\{\text{Arth}[(1 + 4K)/(1 + 8K)^{1/2}] + (t/2\tau_{p^*})(1 + 8K)^{1/2}\}. \quad (18)$$

Here $\text{Arth } x = \tanh^{-1} x = 0.5 \ln[(1 + x)/(1 - x)]$ is the *inverse hyperbolic tangent* [23]. For a limiting case with 100% recycling ($R_{\alpha} = 1$),

$$n_{\alpha}/n_e(R_{\alpha} = 1) = Ct/(1 + 2Ct) = t(n_e\langle\sigma v\rangle_{DT}/4)/[1 + 2t(n_e\langle\sigma v\rangle_{DT}/4)] \quad (19a)$$

or

$$t = (4/n_e\langle\sigma v\rangle_{DT})f_{\alpha}/(1 - 2f_{\alpha}). \quad (19b)$$

For example, for a plasma with $n_e = 10^{20} \text{ m}^{-3}$, $T \approx 10 \text{ keV}$, the time it takes to reach a given level (n_{α}/n_e) of helium ash is $t \text{ (s)} \approx 360f_{\alpha}/(1 - 2f_{\alpha})$, which is about 20 s for 5% and 45 s for 10%. Note that the ash accumulation time t is inversely proportional to nT^2 . Thus, at higher n and T , ash buildup is rather fast, limiting the burn to a few tens of seconds if an active ash removal scheme is not implemented. For $R_{\alpha} \ll 1$, characteristic buildup times, depending on the pumping rate $(1 - R_{\alpha})$, can be relatively

long, permitting steady-state burns. General results can be obtained from Eq. (18) if the particle transport is known or if it can be expressed in terms of τ_E (such as $\tau_p \sim 5\tau_E$). It should be noted that, while the simplified estimates given here are useful in providing qualitative answers to the questions raised earlier, recycling is an edge (not a global) phenomenon, and accurate treatment of the problem requires multidimensional transport analysis.

IV.B. Global Analysis

The sensitivity of performance in TIBER-II plasma to thermal alpha accumulation has been assessed using a simple zero-dimensional power balance model [5–7]. The model used has been benchmarked against 1-1/2-D WHIST transport code results. The physics assumptions are summarized in Table II. Model equations used for the power balance are given in Refs. [5–7]; for completeness, we briefly discuss them here. For a 50-50 D-T plasma, by taking $T_e \approx T_i \approx T$, assuming plasma profiles of the form $x = x_0(1 - r^2/a^2)^{\alpha_x}$ ($x = n, T, J$, with $\alpha_n = 0.5$ and $\alpha_T = 2\alpha_J/3 = 1$), and averaging the power balance equation over the plasma cross section, we obtain (in MW/m⁻³)

$$\begin{aligned} F = 0 &= \langle -P_{\text{con}} - P_B + P_\alpha + P_{\text{OH}} + P_{\text{aux}} \rangle / V \\ &= -0.48 \langle n_{20} \rangle^2 \langle T_{10} \rangle / \langle n_{20} \tau_E \rangle - K_B \langle n_{20} \rangle^2 \langle T_{10} \rangle^{1/2} \\ &\quad + K_\alpha \langle n_{20} \rangle^2 \langle T_{10} / 0.75 \rangle^S + K_{\text{OH}} \langle T_{10} \rangle^{-3/2} + P_{\text{aux}} / V, \end{aligned} \quad (20)$$

where $V = 2\pi^2 a^2 R_0 \kappa \approx 91.4 \text{ m}^3$, $\langle n_{20} \rangle = \langle n_e / 10^{20} \text{ m}^{-3} \rangle$, $\langle T_{10} \rangle = \langle T / 10 \text{ keV} \rangle$, and

$$K_B = 1.8 \times 10^{-2} [1 + 2f_\alpha + Z(Z-1)f_z] = K_B(Z_{\text{eff}} = 1) [1 + 2f_\alpha + Z(Z-1)f_z],$$

$$K_\alpha = 0.14(1 - 2f_\alpha - Zf_z)^2 = K_\alpha(Z_{\text{eff}} = 1) (1 - 2f_\alpha - Zf_z)^2,$$

$$K_{\text{OH}} = 1.28 \times 10^{-2} [1 + 2f_\alpha + Z(Z-1)f_z]$$

$$= K_{\text{OH}}(Z_{\text{eff}} = 1) [1 + 2f_\alpha + Z(Z-1)f_z].$$

$f_\alpha = n_\alpha/n_e$ = fractional thermal alpha density,

$f_z = n_z/n_e$ = fractional impurity density for a single impurity of charge Z ,

$\tau_E = [(1/\tau_{EOH})^2 + (1/\tau_{Eaux})^2]^{-1/2}$ with $\tau_{EOH} = \tau_{ENA}$ and $\tau_{Eaux} = \tau_{EKG}$,

$\tau_{ENA} = 0.07 \langle n_{20} \rangle a R_0^2 q_*$: neo-Alcator [10–13],

$\tau_{EKG} = 0.056 f_L^{1.24} (P_{heat})^{-0.58} R_0^{1.65} a^{-0.49} k^{0.28} \langle n_{20} \rangle^{0.26} B^{0.09} (A_i/1.5)^{0.5}$:

Kaye-Goldston (L-mode $f_L = 1$, H-mode $f_L = 2$) [13],

$$P_{heat} = P_\alpha + P_{OH} + P_{aux} - P_B.$$

Here K_{OH} is evaluated for the TIBER-II parameters and $s = 3$ (2) for $T_{10} < 0.75$ (> 0.75).

IV.C. Discussion of Results

Figure 8 shows the ignition contours for various L-mode enhancement factors of a combined Kaye-Goldston and neo-Alcator scaling in the TIBER-II machine. These contours were obtained from the global power balance equation, Eq. (20), considering the following three separate conditions: (1) there were no impurity or thermal alpha particles ($Z_{eff} = 1$); (2) $Z_{eff} = 1.5$ was maintained with carbon ($Z = 6$) as the only impurity; and (3) thermal alpha concentration in the plasma was maintained at a constant 5% ($= n_\alpha/n_e$) level, corresponding to $Z_{eff} = 1.1$. Reference density ($\langle n_{mu} \rangle / 10^{20} \text{ m}^{-3}$) ~ 1.2 ; ($\langle n_{GR} \rangle / 10^{20} \text{ m}^{-3}$) ~ 2.75) and beta ($\langle \beta_{tot} \rangle \approx \beta_{crit} \sim 6\%$) limits are also shown in Fig. 8 to indicate the extent (in density and temperature) of the operational boundaries. Note that the effect on ignition of the carbon impurity with $Z_{eff} = 1.5$ is nearly identical to the effect of 5% thermal alphas. This observation can easily be made from Eq. (20). At ignition ($P_{aux} = 0$), the contributions from (bremsstrahlung) radiation (P_B) and ohmic heating (P_{OH}) are relatively small in comparison to the conduction (P_{con}) and alpha (P_α) power. The conduction losses are independent of f_α and f_z through the definitions of $\langle n \rangle$, the volume-averaged density, and $\langle T \rangle = \langle n_e T_e + n_i T_i \rangle / \langle 2n_e \rangle$, the density-weighted average temperature. P_α is

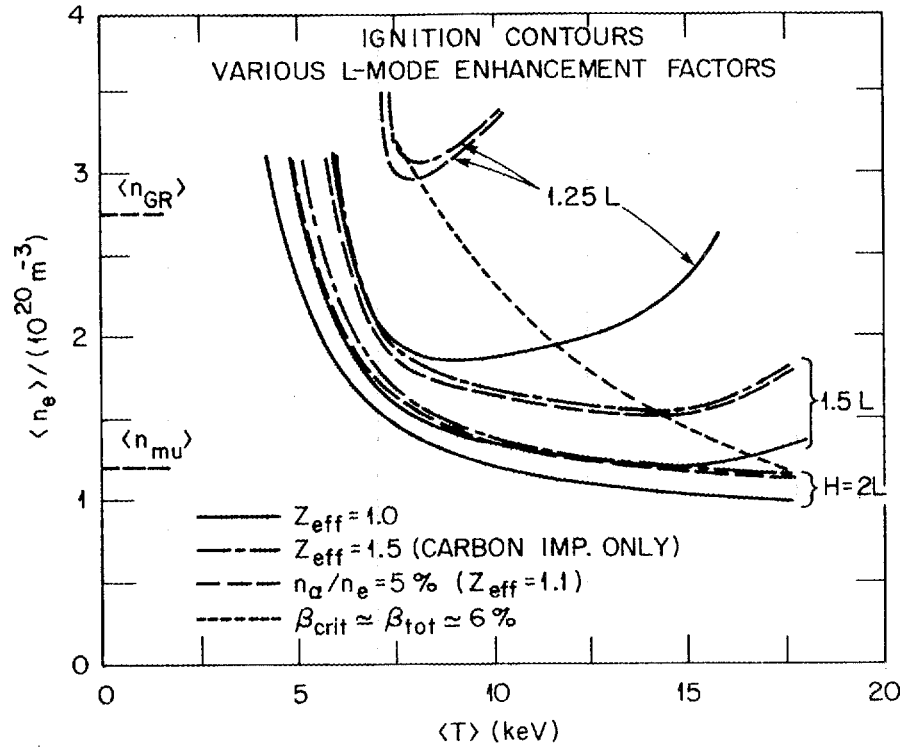


FIG. 8. TIBER-II ignition contours with various L-mode enhancement factors for a combined Kaye-Goldston + neo-Alcator scaling with $Z_{\text{eff}} = 1$ (solid curves), $Z_{\text{eff}} = 1.5$ (due only to carbon impurity — long-and-short dashed curves), and $n_\alpha/n_e = 5\%$ ($Z_{\text{eff}} = 1.1$ due only to thermal alphas — dashed curves). Reference beta ($\sim 6\%$) and density ($\langle n_{20\text{mu}} \rangle \sim 1.2$; $\langle n_{20\text{GR}} \rangle \sim 2.75$) limits are shown to indicate the extent of the operational boundaries. The effect on ignition of the carbon impurity with $Z_{\text{eff}} = 1.5$ is nearly identical to the effect of 5% thermal alpha (ash) population.

proportional to $f_{DT}^2 = (1 - 2f_\alpha - Zf_z)^2$, which yields similar answers if $2f_\alpha \approx Zf_z = (\Delta Z_{\text{eff}})_{\text{imp}} / (Z - 1) = [(Z_{\text{eff}})_{\text{imp}} - 1] / (Z - 1)$.

Figure 9 shows the influence of thermal alpha concentration ($n_\alpha/n_e = 0\text{--}20\%$) on the ignition capability of TIBER-II with an H-mode scaling. Reference beta ($\sim 6\%$) and

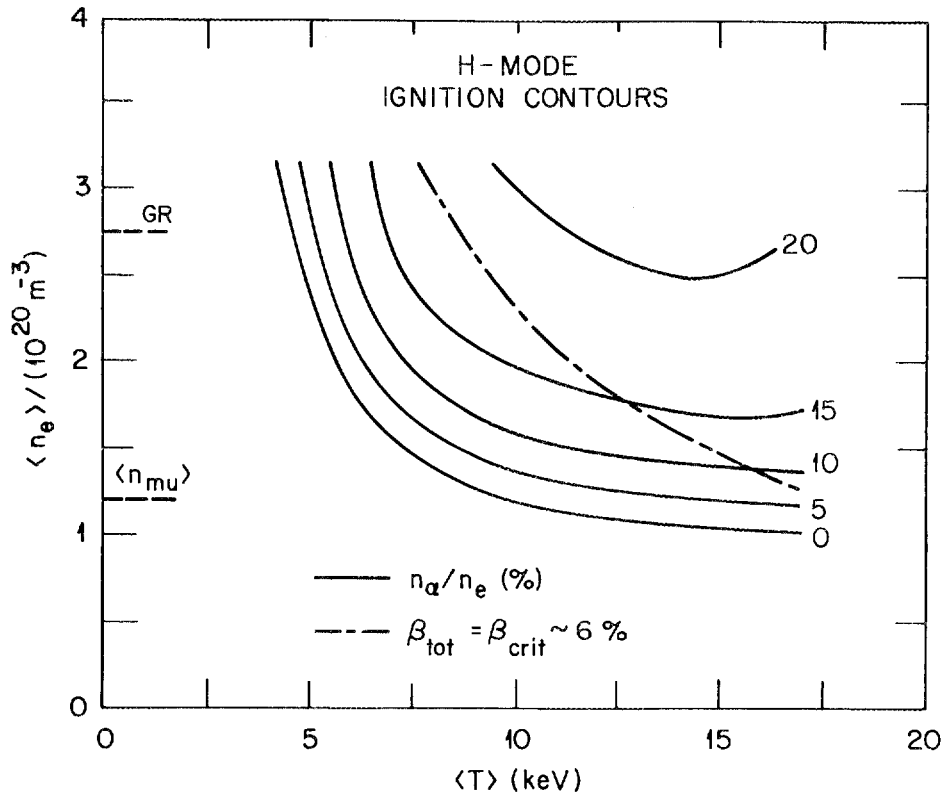


FIG. 9. Influence of thermal alpha concentration (0–20%) on ignition in TIBER-II with an H-mode scaling. Reference beta ($\sim 6\%$) and density ($\langle n_{20\mu} \rangle \sim 1.2$; $\langle n_{20\text{GR}} \rangle \sim 2.75$) limits are shown. Increasing the amount of thermal alphas (ash) moves the ignition contours to higher densities and eventually eliminates the ignition window within the operational boundaries.

density ($\langle n_{20\mu} \rangle \sim 1.2$; $\langle n_{20\text{GR}} \rangle \sim 2.75$) limits are shown. Increasing the amounts of thermalized alphas (ash) moves the ignition contours to higher densities and eventually eliminates the ignition window within the operational boundaries.

V. SUMMARY

Understanding the confinement behavior of both fast and thermal alphas will be a key to the successful operation of any steady-state fusion device. The long classical thermalization time for fast alphas in ETRs (0.5–1.0 s in the core) leads to a significant contribution to the plasma pressure ($\beta_{f\alpha}/\beta_{th} \approx 20\text{--}30\%$ in the core) and a vulnerability of the fast alphas to radial transport during the thermalization process (when $D_\alpha = D_{th} \approx 0.1\text{--}0.5 \text{ m}^2/\text{s}$). The critical issues for fast alphas, then, are the contribution of fast alpha population to the plasma beta limit, the influence of instabilities and turbulence on alpha thermalization, and radial transport of energetic alphas.

Thermal alpha accumulation dilutes the fuel like any other impurity and reduces fusion power production. In ETR it can take a long time for a steady state to be reached (20 s for $n_\alpha/n_e \approx 5\%$ and 45 s for $n_\alpha/n_e \approx 10\%$ with no ash removal). The critical issues for thermal alphas are transport processes, recycling behavior, and pumping capabilities.

To some extent, these issues can be addressed by examining single-particle behavior in machines such as the Joint European Torus and the Tokamak Fusion Test Reactor. Collective phenomena such as instabilities requiring a threshold level of fast alphas (e.g., influence on the beta limit, transport, and thermalization) may be clarified by CIT results. However, the full behavior under steady-state conditions, particularly the issue of ash accumulation, cannot be fully examined until operation of an ETR-scale experiment.

REFERENCES

1. Y. I. KOLESNICHENKO, "The Role of Alpha Particles in Tokamak Reactors," *Nucl. Fusion*, 20, 727 (1980).
2. See papers in *Role of Alpha Particles in Magnetically Confined Fusion Plasmas: Proceedings of the Goteborg Conference, Sweden, June 24-27, 1986*, published in *Physica Scripta* Vol. T16, 1987.
3. See "Near-Term Tokamak Reactors" papers in *Fusion Reactor Design IV (Proc. 4th IAEA Workshop, Yalta, 1986)*, International Atomic Energy Agency, Vienna (1987); also M. A. ABDU et al., "Fusion Reactor Design IV: Conferences and Symposia," *Nucl. Fusion*, 26, 1377 (1986).
4. C. D. HENNING and B. G. LOGAN, eds., "TIBER-II Tokamak Ignition/Burn Experimental Reactor 1986 Status Report," UCID-20863, Lawrence Livermore National Laboratory (1986).
5. N. A. UCKAN and J. SHEFFIELD, "Simple Procedure for Establishing Ignition Conditions in Tokamaks," *Tokamak Startup* (ed. H. Knoepfel), pp. 45-72, Plenum Press, New York (1986); also ORNL/TM-9722, Oak Ridge National Laboratory (1985).
6. N. A. UCKAN, W. A. HOULBERG, and J. SHEFFIELD, "Physics Evaluation of Compact Tokamak Ignition Experiments," *Proc. 11th Symp. Fusion Engineering, Austin, Texas, 1985*, Vol. 1, p. 401 (1986).
7. N. A. UCKAN, "Relative Merits of Size, Field, and Current on Ignited Tokamak Performance: Comparison of CITs and Super-JETs," submitted for publication; also ORNL/TM-10365, Oak Ridge National Laboratory (1987).
8. W. A. HOULBERG, S. E. ATTENBERGER, and L. M. HIVELY, "Contour Analysis of Fusion Reactor Performance," *Nucl. Fusion*, 22, 935 (1982).
9. S. E. ATTENBERGER and W. A. HOULBERG, "Fast Alpha Diffusion and Thermalization in Tokamak Reactors," *Nucl. Technol./Fusion*, 4, 129 (1983).
10. J. SHEFFIELD et al., "Physics Guidelines for the Compact Ignition Tokamak," *Fusion Technol.*, 10, 481 (1986).
11. J. SCHMIDT et al., "A Compact Ignition Experiment," in *Proc. 11th Int. Conf. Plasma Physics and Controlled Nuclear Fusion Research 1986* (Kyoto, 1986), International Atomic Energy Agency, Vienna (1987).

12. See papers (and references therein) in *25 Years of Nuclear Fusion, Anniversary Issue, Nucl. Fusion*, 25, 1011–1194 (1985).
13. S. M. KAYE and R. J. GOLDSTON, "Global Energy Confinement Scaling for Neutral-Beam-Heated Tokamaks," *Nucl. Fusion*, 25, 65 (1985); S. M. KAYE, "A Review of Energy Confinement and Local Transport Scaling Results in Neutral-Beam-Heated Tokamaks," *Phys. Fluids*, 28, 2327 (1985).
14. C. S. CHANG and F. L. HINTON, "Effect of Finite Aspect Ratio on the Neoclassical Ion Thermal Conductivity in the Banana Regime," *Phys. Fluids*, 25, 1493 (1981); "Effect of Impurity Particles on the Finite-Aspect Ratio Neoclassical Ion Thermal Conductivity in a Tokamak," *Phys. Fluids*, 29, 3314 (1986).
15. S. P. HIRSHMAN and D. J. SIGMAR, "Neoclassical Transport of Impurities in Tokamak Plasmas," *Nucl. Fusion*, 21, 1079 (1981).
16. M. MURAKAMI, J. D. CALLEN, and L. A. BERRY, "Some Observations on Maximum Densities in Tokamak Experiments," *Nucl. Fusion*, 16, 347 (1976).
17. M. GREENWALD et al., "A New Look at Density Limits in Tokamaks," PFC/JA-86-22, Plasma Fusion Center, Massachusetts Institute of Technology (1986).
18. F. TROYON, R. GRUBER, H. SAURENMANN, S. SEMENZATO, and S. SUCCI, "MHD-Limits to Plasma Confinement," *Plasma Phys. Controlled Fusion*, 26, 209 (1984).
19. J. G. CORDEY, R. J. GOLDSTON, and D. R. MIKKELSEN, "A Generalized Sufficient Condition for Velocity-Space Stability of Fusion Product Distributions and Application to Heating of D-T Tokamak Reactors," *Nucl. Fusion*, 21, 581 (1981).
20. N. A. UCKAN, W. A. HOULBERG, and J. SHEFFIELD, "Ignition Requirements and Plasma Performance of a High-Field, Small Ignition Device," and "Global Plasma Model Equations for Mission I and Mission II Ignition Studies," unpublished (February 1985).
21. D. A. SPONG, D. J. SIGMAR, and J. J. RAMOS, "Modification of Tokamak Ballooning Stability Boundaries by Alpha Population," *Fusion Technol.* (this issue).
22. K. T. TSANG, D. J. SIGMAR, and J. C. WHITSON, "Destabilization of Low Mode Number Alfvén Waves in a Tokamak by Energetic or Alpha Particles," *Phys. Fluids*, 24, 1508 (1981).
23. For example, see I. S. GRADSHTEYN and I. M. RYZHIK, *Tables of Integrals, Series, and Products*, pp. 57 and 68, 4th ed., Academic Press, New York (1965).

INTERNAL DISTRIBUTION

- | | | | |
|--------|-------------------|--------|---|
| 1-5. | S. E. Attenberger | 23. | T. E. Shannon |
| 6. | L. A. Berry | 24. | J. Sheffield |
| 7. | B. A. Carreras | 25-29. | J. S. Tolliver |
| 8. | R. A. Dory | 30-39. | N. A. Uckan |
| 9. | J. L. Dunlap | 40. | T. Uckan |
| 10. | J. D. Galambos | 41-42. | Laboratory Records Department |
| 11-15. | W. A. Houlberg | 43. | Laboratory Records, ORNL-RC |
| 16. | H. C. Howe | 44. | Document Reference Section |
| 17. | J. F. Lyon | 45. | Central Research Library |
| 18. | M. Murakami | 46. | Fusion Energy Division Library |
| 19. | S. L. Painter | 47-48. | Fusion Energy Division
Publications Office |
| 20. | Y-K. M. Peng | 49. | ORNL Patent Office |
| 21. | R. L. Reid | | |
| 22. | M. J. Saltmarsh | | |

EXTERNAL DISTRIBUTION

50. Office of the Assistant Manager for Energy Research and Development, U.S. Department of Energy, Oak Ridge Operations Office, P. O. Box E, Oak Ridge, TN 37831
51. J. D. Callen, Department of Nuclear Engineering, University of Wisconsin, Madison, WI 53706-1687
52. J. F. Clarke, Director, Office of Fusion Energy, Office of Energy Research, ER-50 Germantown, U.S. Department of Energy, Washington, DC 20545
53. R. W. Conn, Department of Chemical, Nuclear, and Thermal Engineering, University of California, Los Angeles, CA 90024
54. S. O. Dean, Fusion Power Associates, Inc., 2 Professional Drive, Suite 249, Gaithersburg, MD 20760
55. H. K. Forsen, Bechtel Group, Inc., Research Engineering, P. O. Box 3965, San Francisco, CA 94105
56. J. R. Gilleland, L-644, Lawrence Livermore National Laboratory, P.O. Box 5511, Livermore, CA 94550
57. R. W. Gould, Department of Applied Physics, California Institute of Technology, Pasadena, CA 91125

58. R. A. Gross, Plasma Research Laboratory, Columbia University, New York, NY 10027
59. D. M. Meade, Princeton Plasma Physics Laboratory, P.O. Box 451, Princeton, NJ 08544
60. M. Roberts, International Programs, Office of Fusion Energy, Office of Energy Research, ER-52 Germantown, U.S. Department of Energy, Washington, DC 20545
61. W. M. Stacey, School of Nuclear Engineering and Health Physics, Georgia Institute of Technology, Atlanta, GA 30332
62. D. Steiner, Nuclear Engineering Department, NES Building, Tibbetts Avenue, Rensselaer Polytechnic Institute, Troy, NY 12181
63. R. Varma, Physical Research Laboratory, Navrangpura, Ahmedabad 380009, India
64. Bibliothek, Max-Planck Institut für Plasmaphysik, Boltzmannstrasse 2, D-8046 Garching, Federal Republic of Germany
65. Bibliothek, Institut für Plasmaphysik, KFA Jülich GmbH, Postfach 1913, D-5170 Jülich, Federal Republic of Germany
66. Bibliothek, KfK Karlsruhe GmbH, Postfach 3640, D-7500 Karlsruhe 1, Federal Republic of Germany
67. Bibliotheque, Centre de Recherches en Physique des Plasmas, Ecole Polytechnique Federale de Lausanne, 21 Avenue des Bains, CH-1007 Lausanne, Switzerland
68. F. Prévot, CEN/Cadarache, Departement de Recherches sur la Fusion Contrôlée, F-13108 Saint-Paul-lez-Durance Cedex, France
69. Bibliothèque, CEN/Cadarache, F-13108 Saint-Paul-lez-Durance Cedex, France
70. Documentation S.I.G.N., Departement de la Physique du Plasma et de la Fusion Contrôlée, Association EURATOM-CEA, Centre d'Etudes Nucléaires, B.P. 85, Centre du Tri, F-38041 Grenoble, France
71. Library, Culham Laboratory, UKAEA, Abingdon, Oxfordshire, OX14 3DB, England
72. Library, JET Joint Undertaking, Abingdon, Oxfordshire, OX14 3EA, England
73. Library, FOM-Instituut voor Plasmafysica, Rijnhuizen, Edisonbaan 14, 3439 MN Nieuwegein, The Netherlands
74. Library, Institute of Plasma Physics, Nagoya University, Chikusa-ku, Nagoya 464, Japan
75. Library, International Centre for Theoretical Physics, P.O. Box 586, I-34100 Trieste, Italy
76. Library, Centro Ricerca Energia Frascati, C.P. 65, I-00044 Frascati (Roma), Italy
77. Library, Plasma Physics Laboratory, Kyoto University, Gokasho, Uji, Kyoto, Japan

78. Plasma Research Laboratory, Australian National University, P.O. Box 4, Canberra, A.C.T. 2601, Australia
79. Library, Japan Atomic Energy Research Institute, Tokai Research Establishment, Tokai, Naka-gun, Ibaraki-ken 311-02, Japan
80. Library, Japan Atomic Energy Research Institute, Naka Research Establishment, Naka-machi, Naka-gun, Ibaraki-ken, Japan
81. G. A. Eliseev, I. V. Kurchatov Institute of Atomic Energy, P. O. Box 3402, 123182 Moscow, U.S.S.R.
82. V. A. Glukhikh, Scientific-Research Institute of Electro-Physical Apparatus, 188631 Leningrad, U.S.S.R.
83. I. Shpigel, Institute of General Physics, U.S.S.R. Academy of Sciences, Ulitsa Vavilova 38, Moscow, U.S.S.R.
84. D. D. Ryutov, Institute of Nuclear Physics, Siberian Branch of the Academy of Sciences of the U.S.S.R., Sovetskaya St. 5, 630090 Novosibirsk, U.S.S.R.
85. V. T. Tolok, Kharkov Physical-Technical Institute, Academical St. 1, 310108 Kharkov, U.S.S.R.
86. Library, Academia Sinica, P.O. Box 3908, Beijing, China (PRC)
87. R. A. Blanken, Experimental Plasma Research Branch, Division of Applied Plasma Physics, Office of Fusion Energy, Office of Energy Research, ER-542, Germantown, U.S. Department of Energy, Washington, DC 20545
88. K. Bol, Princeton Plasma Physics Laboratory, P.O. Box 451, Princeton, NJ 08544
89. R. A. E. Bolton, IREQ Hydro-Quebec Research Institute, 1800 Montee Ste.-Julie, Varennes, P.Q. JOL 2P0, Canada
90. D. H. Crandall, Experimental Plasma Research Branch, Division of Applied Plasma Physics, Office of Fusion Energy, Office of Energy Research, ER-542, Germantown, U.S. Department of Energy, Washington, DC 20545
91. R. L. Freeman, GA Technologies, Inc., P.O. Box 85608, San Diego, CA 92138
92. K. W. Gentle, RLM 11.222, Institute for Fusion Studies, University of Texas, Austin, TX 78712
93. R. J. Goldston, Princeton Plasma Physics Laboratory, P.O. Box 451, Princeton, NJ 08544
94. J. C. Hosea, Princeton Plasma Physics Laboratory, P.O. Box 451, Princeton, NJ 08544
95. S. W. Luke, Division of Confinement Systems, Office of Fusion Energy, Office of Energy Research, ER-55, Germantown, U.S. Department of Energy, Washington, DC 20545

96. E. Oktay, Division of Confinement Systems, Office of Fusion Energy, Office of Energy Research, ER-55, Germantown, U.S. Department of Energy, Washington, DC 20545
97. D. Overskei, GA Technologies, Inc., P.O. Box 85608, San Diego, CA 92138
98. R. R. Parker, Plasma Fusion Center, NW 16-288, Massachusetts Institute of Technology, Cambridge, MA 02139
99. W. L. Sadowski, Fusion Theory and Computer Services Branch, Division of Applied Plasma Physics, Office of Fusion Energy, Office of Energy Research, ER-541, Germantown, U.S. Department of Energy, Washington, DC 20545
100. J. W. Willis, Division of Confinement Systems, Office of Fusion Energy, Office of Energy Research, ER-55, Germantown, U.S. Department of Energy, Washington, DC 20545
101. A. P. Navarro, Division de Fusion, CIEMAT, Avenida Complutense 22, E-28040 Madrid, Spain
102. Laboratory for Plasma and Fusion Studies, Department of Nuclear Engineering, Seoul National University, Shinrim-dong, Gwanak-ku, Seoul 151, Korea
103. M. A. Abdou, School of Engineering and Applied Science, 6288 Boelter Hall, University of California, Los Angeles, CA 90024
104. C. C. Baker, Argonne National Laboratory, 9700 South Cass Avenue, Argonne, IL 60439
105. C. Bolton, Office of Fusion Energy, Office of Energy Research, ER-55 Germantown, U.S. Department of Energy, Washington, DC 20545
106. D. R. Cohn, Plasma Fusion Center, NW 16-140, Massachusetts Institute of Technology, Cambridge, MA 02139
107. B. Coppi, 77 Massachusetts Avenue, Massachusetts Institute of Technology, Cambridge, MA 02139
108. R. C. Davidson, 77 Massachusetts Avenue, Massachusetts Institute of Technology, Cambridge, MA 02139
109. N. A. Davies, Office of Fusion Energy, Office of Energy Research, ER-55 Germantown, U.S. Department of Energy, Washington, DC 20545
110. S. A. Eckstrand, Office of Fusion Energy, Office of Energy Research, ER-55 Germantown, U.S. Department of Energy, Washington, DC 20545
111. A. J. Favale, MS-A0126, Grumman Corporation, P.O. Box 31, Bethpage, NY 11714
112. T. K. Fowler, L-640, Lawrence Livermore National Laboratory, P.O. Box 5511, Livermore, California 94550
113. H. P. Furth, Princeton Plasma Physics Laboratory, P.O. Box 451, Princeton, NJ 08544
114. C. D. Henning, L-640, Lawrence Livermore National Laboratory, P.O. Box 5511, Livermore, California 94550

115. T. R. James, Office of Fusion Energy, Office of Energy Research, ER-55 Germantown, U.S. Department of Energy, Washington, DC 20545
116. R. A. Krakowski, CTR-12, Mail Stop 641, Los Alamos National Laboratory, P.O. Box 1663, Los Alamos, NM 87545
117. G. L. Kulcinski, Room 439, Department of Nuclear Engineering, Engineering Research Building, University of Wisconsin, 1500 Johnson Drive, Madison, WI 53706
118. B. G. Logan, L-644, Lawrence Livermore National Laboratory, P.O. Box 5511, Livermore, California 94550
119. J. A. Maniscalco, R1/2128, TRW Defense and Space Systems, One Space Park, Redondo Beach, CA 90278
120. G. H. Miley, Nuclear Engineering Department, University of Illinois, Urbana, IL 61801
121. D. B. Montgomery, Plasma Fusion Center, NW 16-140, Massachusetts Institute of Technology, Cambridge, MA 02139
122. D. E. Post, Princeton Plasma Physics Laboratory, P.O. Box 451, Princeton, NJ 08544
123. P. H. Rebut, JET Joint Undertaking, Abingdon, Oxon OX14 3EA, England
124. F. L. Ribe, College of Engineering, FL-10, AERL Bldg., University of Washington, Seattle, WA 98195
125. D. Ross, Fusion Research Center, The University of Texas, Austin, TX 78712
126. P. H. Rutherford, Princeton Plasma Physics Laboratory, P.O. Box 451, Princeton, NJ 08544
127. J. A. Schmidt, Princeton Plasma Physics Laboratory, P.O. Box 451, Princeton, NJ 08544
128. R. D. Stambaugh, GA Technologies, Inc., P.O. Box 85608, San Diego, CA 92138
129. P. M. Stone, Office of Fusion Energy, Office of Energy Research, ER-55 Germantown, U.S. Department of Energy, Washington, DC 20545
130. H. Weitzner, Courant Institute of Mathematical Sciences, New York University, 251 Mercer Street, New York, NY 10012
- 131-207. Given distribution as shown in TIC-4500, Magnetic Fusion Energy (Distribution Category UC-20)

